Chapter 5

Spectral broadening and ultrashort pulse generation in hollow fibers

In this chapter, the use of noble-gas-filled hollow fibers as systems for the generation of ultrabroad spectra and ultrashort pulses is considered. The theoretical consideration of SPM, which is the main broadening mechanism in this case, is given in Chapter 2.

Optical pulse compression by self-phase modulation (SPM) in hollow waveguides filled with noble gases as nonlinear media [36, 97] has recently attracted large interest for the generation of the presently shortest optical pulses with a duration of 4-5 fs and pulse energies of mJ. The aim to reduce this pulse duration down to the single or even sub-cycle region raises several questions concerning the characteristics and limitations of ultra-wide spectral broadening by SPM, the frequency-dependence of the spectral phase during propagation and possible improvements of this method. Addressing these

questions, in the present Chapter we study spectral broadening by SPM in hollow waveguides theoretically and find the optimal input parameters and compressor design. As a result, we show, to the first time in our knowledge, that in hollow waveguides generation of ultrawide spectra covering almost three octaves from 1600 nm up to 250 nm is possible for a pressure where the group velocity dispersion (GVD) is weak and anomalous in a large wavelength range. Compensation of the predicted smooth spectral phase by a broadband liquid crystal spatial light modulator (LC SLM) results in sub-cycle pulses with a duration of about 1.5 fs. The predicted regime shows similarities with two-octave spectral broadening recently observed in photonic [8] and tapered [10] fibers. The distinct advantage of hollow fibers is the possibility to increase the pulse energy by five orders of magnitude up to the mJ level. Additionally, we study spectral broadening by SPM for normal pressure and cross-phase modulation in hollow waveguides and find good agreement with experimental measurements. In other related works sub-cycle pulse compression by SPM in fused-silica fibers [14] and by high-order stimulated Raman scattering in H_2 [46] has been examined.

5.1 Choice of pulse and waveguide parameters

Several considerations define the range of parameters in which the effect of self-phase modulation can yield ultrabroad spectra. The width of the radiation generated by the effect of SPM is given by

$$\Delta\omega_{\mathrm{SPM}} = 1.39 pW(\omega_0) n_2 I_0 \frac{\omega_0 L}{c\tau_0}, \tag{5.1}$$

where p is the pressure of the gas in the hollow fiber, I_0 is the input intensity, and L is the propagation length. This expression, however, does not take the effects of dispersion into account. With propagation, the duration of the pulse will increase thus reducing peak intensity and the SPM-caused broadening. Therefore the propagation length is effectively limited by the value $\tau_0^2/\beta''(\omega_0)$ or even shorter because of the change in the pulse spectrum during the propagation. Another source of limitation imposed on the propagation length is loss, with maximum effective propagation length $z_{eff,m}$ being given by

$$z_{eff,m} = 2\pi\omega^2 a^3 \sqrt{1-\nu^2}/([1+\nu^2]2.405^2 c^2). \qquad (5.2)$$

In the case of typical 100-μm radius fibers these lengths equals around 3 m. The initial pulse duration should be chosen as short as possible to achieve broader spectra. Here we limit ourselves not by the record values but by more available 15 fs initial duration. With this duration the typical effective propagation length as determined by the dispersion is also of the order of several meters. Therefore further consideration is limited to the waveguides with a maximum of 2.8 m length. The input wavelength is determined by the Ti:sappphire laser to be 830 nm. Thus the only unknown parameter in the formula for the SPM-induced spectral broadening is the input intensity.

Two effects limit the maximum intensity: self-focusing and ionization. In a medium with nonlinear properties, the modification of the refractive index in the transverse direction causes focusing of the beam in the case of positive n_2. For sufficiently intense beams that can cause self-focusing to overcome diffraction and lead to collapse of the beam accompanied by ionization. In the free propagation Gaussian beam the critical power which demarcates the

self-focusing is given by $\lambda_0^2/(2n_2)$. In guiding systems such as hollow fibers, the self-focusing leads to the energy transfer from the fundamental mode to the higher transverse modes. This effect can be neglected [27, 98] for intensity lower than $0.25\lambda/(\pi n_2)$. For argon at atmospheric pressure, this yields 107 TW/cm^2 for a=100 μm. To estimate the effect of the ionization on the propagation of the pulse and spectral broadening, we consider the ionization rate as described by the Ammosov-Delone-Krainov model for neutral atoms:

$$\frac{\partial n_e}{\partial t} = \left(\frac{3m_e e^4}{\pi \hbar^3 n_*^{4.5}} \right)^{1/2} \left(\frac{4}{\mathcal{E} n_*^4} \right)^{2n_* - 1.5} \exp\left(-\frac{2}{3n_*^3 \mathcal{E}} \right) \tag{5.3}$$

where $\mathcal{E} = E/E_{bs}$ is the renormalized electric field, e is the electron charge, $n_* = (2I\hbar^2/(m_e e^4)^{1/2}$ with I being the ionization potential, e is the electron charge, m_e is the electron mass, and $E_{bs} = 5.142 \times 10^{11}$ V/m is the electric field at Bohr radius in hydrogen atom. For any pulse shape $E(t)$, including spectrally ultrabroad pulses, the number of free electrons can be calculated by means of this expression. In Fig. 5.1, the dependence of the $\Delta n = n - 1$ for the different contributions (linear, nonlinear as well as $|\Delta n| = 2n_e \pi e^2/(m_e \omega^2)$ caused by free electron contribution) are shown as a function of intensity.

For ionization to be negligible, we assume that its contribution to polarization is one order of magnitude less than that of nonlinear polarization. This corresponds to intensities less than 105 TW/cm^2.

The expression (5.3) explains why noble gases are the best alternative for the gas filling in the hollow fibers: they have higher ionization potential and therefore can sustain higher intensities without producing undesirable free-electron plasma. Among the noble gases, the relation between the nonlinear refractive index n_2, linear dispersion a given by $\beta''(\omega_0)$ as well as ionization potential establishes argon as the best gas filling.
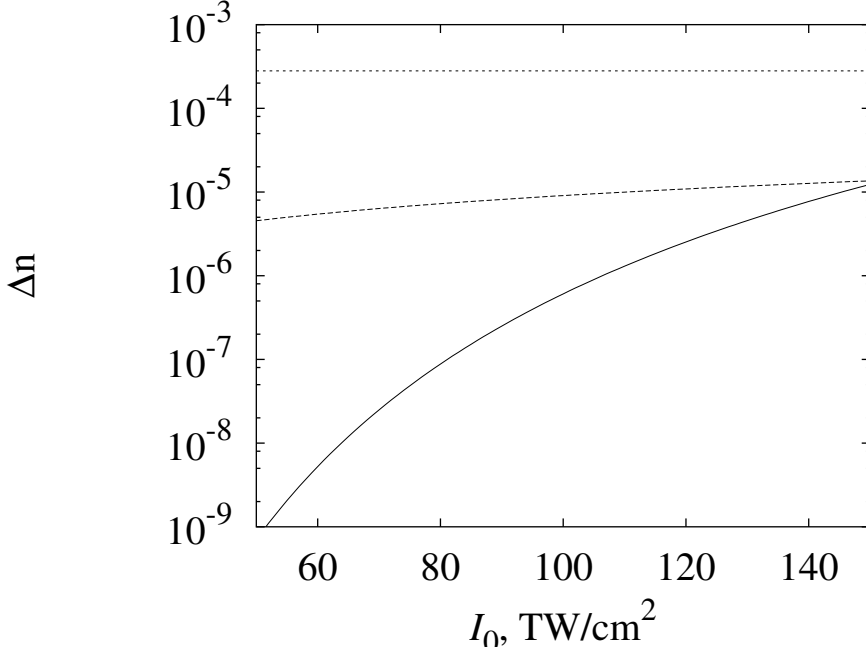
Figure 5.1: Dependence of the linear (dotted), nonlinear (dashed), and ionization-caused (solid) change of the refractive index versus intensity for argon at $p=1$ atm.

5.2 Results of numerical simulation and discussion

After propagation through the hollow waveguide the pulses can be compressed by linear optical elements with controlled dispersion. The Fourier-transformed field after the compressor is

$$E_c(\omega) = |E(\omega)| \exp[i\phi(\omega) - i\phi_c(\omega)], \qquad (5.4)$$

where $\phi(\omega)$ is the pulse phase at the waveguide output and $-\phi_c(\omega)$ is the frequency-dependent phase introduced by the compressor. Here we consider the compression by a LC SLM and model its action in the following way:

the transmission range of the modulator between 0.415 μm and 1.66 μm is split into 256 channels. Within every channel, the quantity ϕ_c is the mean pulse phase within the spectral range of this channel. In comparison, an ideal compressor compensates the pulse phase exactly: $\phi_c(\omega) = \phi(\omega)$.

First we study propagation of pulses with initial center wavelength $\lambda = 2\pi c/\omega_0 = 830$nm and duration τ_0 through a waveguide filled with argon for normal pressure $p =$1 atm. The propagation is described by the basic equation (2.66), which is solved numerically. The Sellmeyer fit parameters for argon are $a_1 = 0.105$ fs^{-2}, $\omega_1 = 19.5$ fs^{-1}, $a_2 = 0.760$ fs^{-2}, $\omega_2 = 51.2$ fs^{-1} for the pressure $p=$1 atm and $\chi_3=3.48\times10^{-26}$ m^2/V^2 [99]. In Fig. 5.2 the pulse spectra, the pulse phases and the pulse shapes at the output of the waveguide and the compressor are presented for parameters given in the caption. The spectra show a red-shift of the maxima and are extended from 1100 to 550 nm for the input intensity $I = \epsilon_0 cE^2/2 =$20 TW/cm^2 and from 1400 to 400 nm for $I =$60 TW/cm^2. The pulse phases presented in Fig. 5.2(b) by solid lines show a smooth behavior and result in a chirp of the pulse. For comparison, the dotted lines represent the linear phase

$$\phi_L(\omega) = \sqrt{1 + \chi_B(\omega) + \chi_{WG}(\omega)}\,\omega L/c \qquad (5.5)$$

of the bulk and waveguide contribution for a pulse with a small intensity. The calculated results are in good agreement with experimental measurements of Ref. [97], where for the same input and waveguide parameters as in case II in Fig. 5.2(a) a spectrum over the range of 400-1100 nm was observed. Besides, we calculate the interferometric autocorrelation trace for $E(\eta)$ and also find good agreement with the FWHM of the corresponding measurements. We also obtain good agreement with the results in Ref. [36], where for $p =$3.3
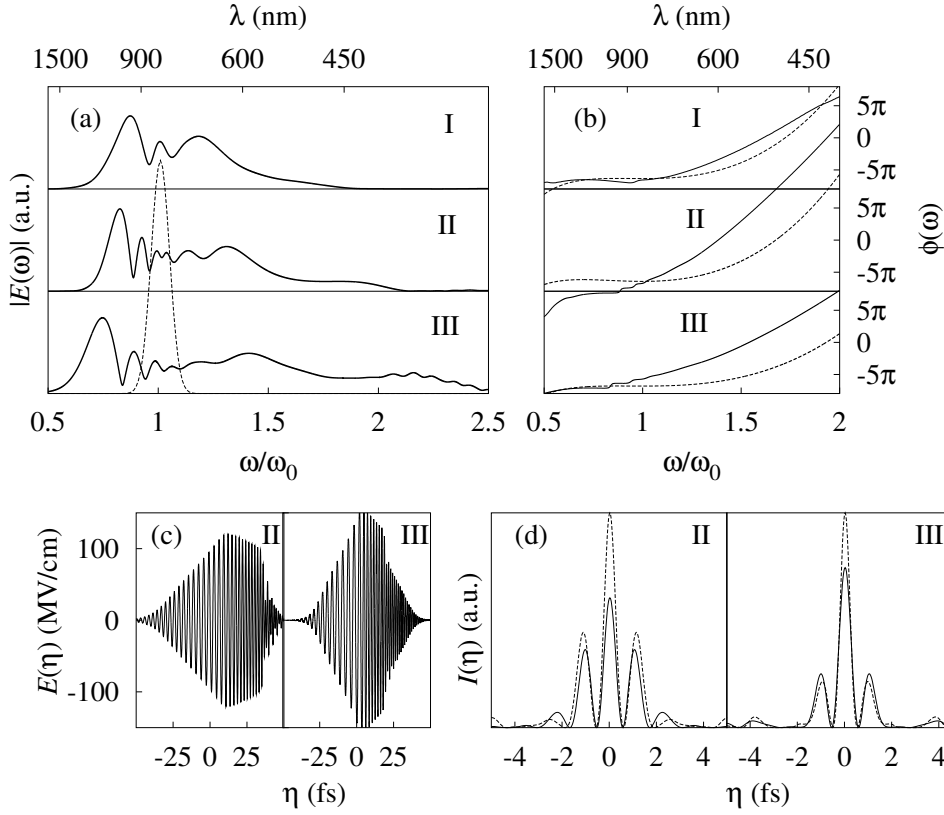
Figure 5.2: Pulse characteristics after propagation for normal pressure of 1 atm. Part (a) shows output spectra (solid) and input spectrum (dotted), (b) pulse phases (solid) and linear phases (dotted), temporal shapes (c) after the waveguide and (d) after the LC SLM (solid) and the ideal compressor (dotted). The parameters are (I) $I = 20$ TW/cm^2, $\tau_0 = 15$ fs, $z = 90$ cm, $a = 100$ μm; (II) $I = 35$ TW/cm^2, $\tau_0 = 25$ fs, $z = 90$ cm, $a = 125$ μm; (III) $I = 60$ TW/cm^2, $\tau_0 = 15$ fs, $z = 50$ cm, $a = 100$ μm.

atm, $z = 60$ cm and $I = 41$ TW/cm^2 compressed pulses with a duration of 5.3 fs were obtained. The results in Fig. 5.2 predict that for a two times higher input intensity as used in these both experiments the spectrum is extended to wavelengths as short as 330 nm. To estimate the pulse duration

for the corresponding shortened pulses in case III in Fig. 5.2(d) we determine the envelope by fitting $I(\eta)$ with the product of a Gaussian envelope and a harmonic function and find a FWHM of the envelope of 1.6 fs for compression by a LC SLM. However, the possible enlargement of the input intensity is limited by the onset of ionization and by the coupling to higher transverse modes.

With relation to the results presented, the questions arise whether spectra broader than that shown in Fig. 5.2 can be achieved by SPM in hollow waveguides and whether it is possible to obtain sub-cycle pulses with lower initial intensity. To find an optimum regime for supercontinuum generation for intensities below the above discussed intensity thresholds the sensitive influence of dispersion and its possible control has to be studied. Due to the anomalous waveguide contribution to P_L in hollow fibers, the zero-GVD wavelength can be controlled by the pressure. The dependence of the GVD parameter $D = \partial^2 \phi_L(\omega)/\partial\omega^2$ versus the wavelength is depicted in Fig. 5.3 for different pressures of argon in a waveguide with radius a=100 μm. For λ =830 nm the GVD is zero at p =0.755 atm and a small GVD parameter in a large wavelength range can be achieved below this pressure.

In Fig. 5.4 the results are presented for the pressure p =0.3 atm and p =0.5 atm, for which the GVD parameter is small over the generated spectrum. Although the nonlinear refractive index for the lower pressure is about three times smaller than that for normal pressure the spectral components in cases II and III in Fig. 5.4(a) extend up to 250 nm and therefore the spectrum contains almost three octaves. The observed FWHM spectral width
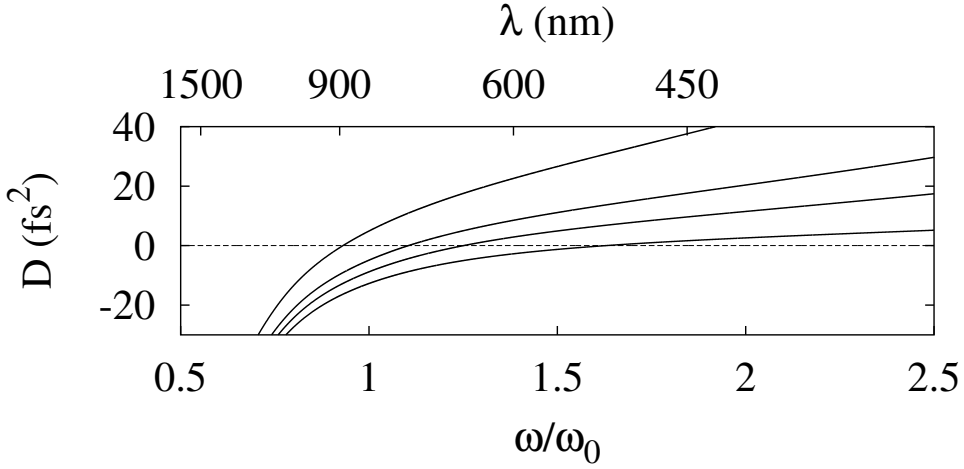
Figure 5.3: GVD parameter D versus frequency for $a = 100\ \mu$m, $L = 1$ m, and a pressure equal to 1, 0.5, 0.3, 0.1 atm (from top to bottom).

Δ_ω/ω correspond to the theoretical prediction [50]

$$\Delta\omega/\omega = 1.37 n_2 I z/(\tau_0 c) \tag{5.6}$$

for SPM-induced spectral broadening. For example, for case I in Fig. 5.4 the numerical width is 1 and theoretical prediction is 1.3. This supercontinuum is even broader than in photonic [8] and tapered [10] fibers recently observed, but here the pulse energy is five orders of magnitude higher due to the much greater diameter. The pulse phase presented in Fig. 5.4(b), case II by the solid line shows an almost linear dependence on the frequency between 250 nm and 830 nm, whereas outside this range the pulse phase nonlinearly depends on the frequency. The temporal shape of the pulse at the output of the waveguide for the parameters of case II is shown in Fig. 5.4(c), where the self-steepened back front containing the high-frequency spectral part and a flat triangle-like leading front are visible. Note that this pulse shape is qualitatively different from the nearly triangular pulse shape with a steep
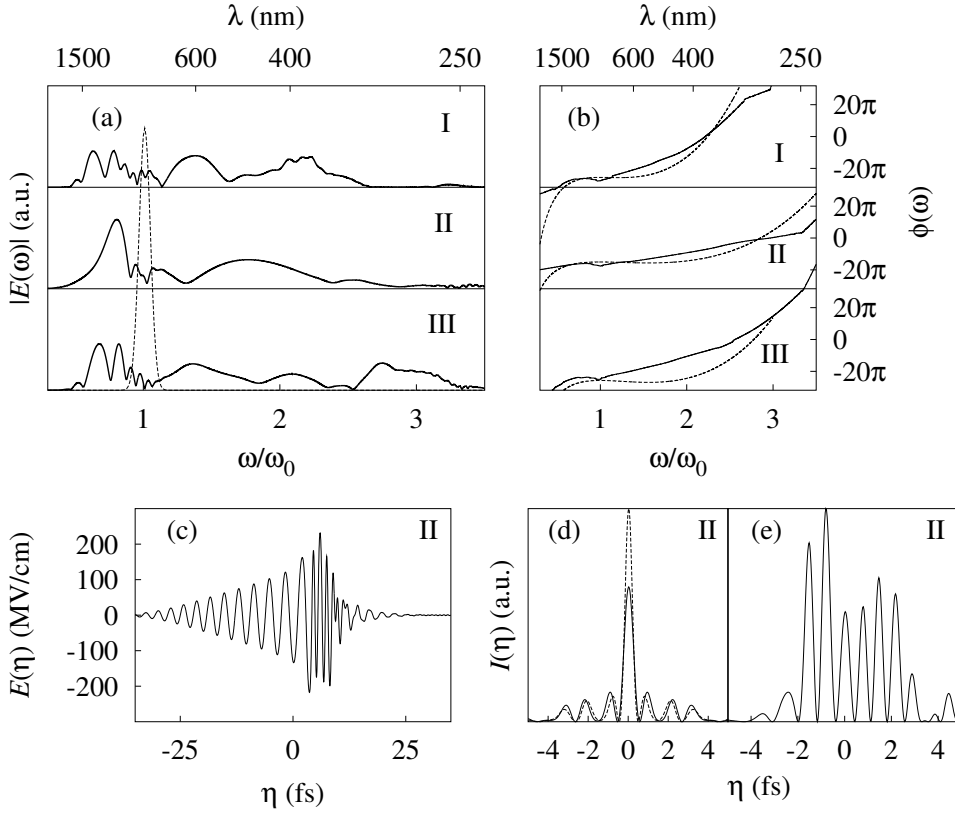
Figure 5.4: Pulse propagation characteristics for optimized pressure. Part (a) shows output spectra (solid) and the input spectrum (dotted), (b) pulse phases (solid) and linear phases (dotted), temporal shapes (c) after the waveguide, (d) after the LC SLM (solid) and ideal compressor (dotted) and (e) after a spectral filter. The parameters are $a = 100$ μm, $\tau_0 = 15$ fs and (I) $I = 35$ TW/cm^2, $z = 2.5$ m, $p = 0.5$ atm; (II) $I = 50$ TW/cm^2, $z = 1$ m, $p = 0.3$ atm; (III) $I = 50$ TW/cm^2, $z = 2$ m, $p = 0.3$ atm.

leading front in the case of fused silica with large normal dispersion [14]. The pulses after passage through an ideal (dotted line) and a LC SLM compressor (solid line) are shown in Fig. 5.4(d). The estimated pulse duration is 1.5 fs for the compression by a LC SLM. This duration is less than the period of the

carrier ($\sim$2.4 fs) and therefore the obtained shortened pulse is a sub-cycle pulse. The predicted linear dependence of the pulse phase on the frequency over a significant part of the spectrum raises the question whether the pulse can be shortened without additional phase control by a simple filter which would cut off the spectrum outside this part. As can be seen in Fig. 5.4(e), a shortened pulse with a duration of about 5 fs with a mean wavelength of 390 nm is obtained in this way. Note that this pulse is shorter than the current experimental record [100] of 8 fs at this central wavelength.

An ultra-wide spectrum over two octaves can also be realized for a lower intensity. In the upper section of Fig. 5.5 the results for an input intensity of 20 TW/cm^2 at the pressure of 0.3 atm are presented. In this case the spec-
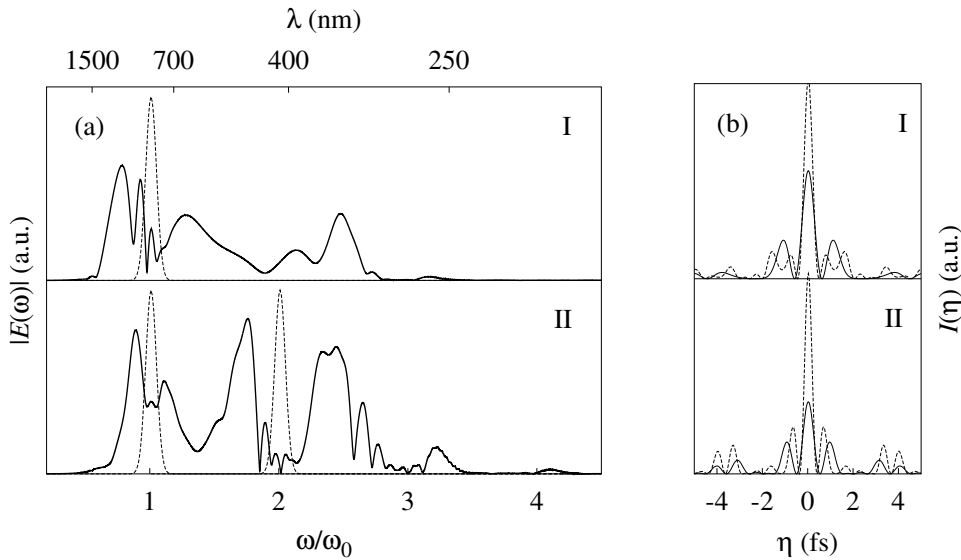

Figure 5.5: (a) Spectra and (b) temporal shapes after a LC SLM (solid) and an ideal compressor (dotted). Parameters are τ_0=15 fs, I =40 TW/cm^2, a =100 μm and (I) p =0.3 atm, z =2.5 m; (II) p =0.187 atm, z =2.8 m with fundamental and second-harmonic inputs.

trum extends up to 300 nm, which is significantly broader than for normal pressure as presented in Fig. 5.2(a), case I. The pulse after compression by a LC SLM plotted in the upper part of Fig. 5.5(b) has a duration of 1.9 fs. Finally, we study the propagation of two synchronized pulses with the same intensity of 20 TW/cm^2, 15 fs duration and wavelengths of 830 and 415 nm. For an enhancement of cross-phase modulation and degenerate four-wave mixing we choose the pressure at which the group velocities of both input pulses are equal. In Fig. 5.5(a) the pulse shape after the waveguide and in Fig. 5.5(b) the shortened pulses after the compressor are presented. As seen by comparison of both curves in Fig. 5.5 this scheme, recently studied in Ref. [101], does not give an advantage compared with the case of a single pulse with optimized pressure and the same input intensity, but it is more difficult to realize experimentally and the waveguide losses are 57% of input energy at 830 nm. A narrower spectrum was observed for $p =$ 3.3 atm using cross-phase modulation by two pulses with fundamental and second-harmonic frequencies and similar input and waveguide parameters [101].

In conclusion, the propagation of short intense pulses in hollow waveguides is studied theoretically without the use of SVEA. By choosing such a pressure that the GVD parameter is small in a large wavelength range, we predict a regime of supercontinuum generation with spectra covering almost three octaves. This allows the generation of sub-cycle pulses by an appropriate broadband modulator for chirp compensation. Additionally, we obtain 5-fs pulses in the UV range using an amplitude filter.